Mode-locking pulse dynamics in a fiber laser with a saturable Bragg reflector

J. Nathan Kutz*

Program in Applied and Computational Mathematics, Princeton University, Princeton, New Jersey 08544

Brandon C. Collings and Keren Bergman

Department of Electrical Engineering and Advanced Technology Center for Photonics and Opto-Electronic Materials, Engineering Quadrangle, Princeton University, Princeton, New Jersey 08544

Sergio Tsuda, Steven T. Cundiff, and Wayne H. Knox

Bell Laboratories, Lucent Technologies, 101 Crawfords Corner Road, Holmdel, New Jersey 07733

Philip Holmes and Michael Weinstein†

Program in Applied and Computational Mathematics, Princeton University, Princeton, New Jersey 08544

Received December 20, 1996; revised manuscript received March 28, 1997

A theoretical model is developed for the pulse dynamics in a fiber laser mode locked by a saturable Bragg reflector and operating in regimes beyond the scope of the master mode-locking equation. An asymptotically valid mode-locked evolution equation is derived, which includes a heuristic model for the saturable Bragg reflector dynamics. The model employed allows, for the first time to our knowledge, direct comparison (with no free parameters) of the theoretical predictions of the pulse spectral and temporal profiles with experimental results in both the normal and anomalous dispersion regimes. Extensive numerical simulations of the governing evolution equation, an averaged equation, and analytical solutions are found to be in excellent agreement with experimental results. © 1997 Optical Society of America [S0740-3224(97)04010-1]

1. INTRODUCTION

Compact sources of optical pulses near wavelengths of 1.55 μm are key enabling technologies for high-speed fiber-optic communication systems and interconnection networks. Erbium-doped mode-locked fiber lasers, currently the subject of much research, provide a potentially attractive short-pulse source.[1] Various fiber lasers have been demonstrated that use passive mode-locking techniques operating in both the normal and anomalous dispersion regimes. Passive mode locking has been successfully achieved by several groups employing additive-pulse mode locking (APM), which converts nonlinear self-phase modulation to ultrafast amplitude modulation with an interferometer in the figure-eight laser[2–4] or by polarization rotation in the ring laser.[5,6] The mode-locking force of APM is in essence equivalent to a fast saturable absorber. Fiber lasers have also been passively mode locked in a linear-cavity configuration that employs a semiconductor structure for the fast saturable absorber.[7,8]

A recently developed semiconductor saturable absorber device incorporates an epitaxially grown pair of InGaAs quantum wells and a low-loss Bragg reflector structure to produce a saturable Bragg reflector (SBR).[9] This nonlinear mirror has been used to passively mode lock Cr^{+4}:YAG, Ti:sapphire, Cr:LiSAF, and erbium-doped fiber lasers near 1.55 μm.[8,10] Similar ultrafast semiconductor saturable absorbers have been developed that incorporate high- and low-finesse Fabry–Perot structures and have been successfully used to passively mode lock lasers at other wavelengths.[11] The advantage of semiconductor saturable absorbers over other passive mode-locking techniques such as Kerr lens mode locking or APM is their extremely low saturation energies, permitting efficient femtosecond mode locking of low-gain-coefficient or short-gain-length lasers. Erbium-doped fiber lasers mode locked with the SBR have achieved higher repetition rates (by factors of 3 or more) than APM mode-locked fiber lasers in a single pulse per round-trip configuration. These results are promising for high-speed networks that require broadband and stable sources.

Although significant strides have been made toward a complete description of femtosecond mode locking in solid-state lasers,[1,12] thus far passive mode locking in a fiber laser has been studied with Haus' master mode-locking equation[13–16] or as a soliton system under perturbation.[17–19] The master equation is derived under the condition that nonlinear changes to the intracavity pulse must be small per round trip. In the soliton perturbation approach the pulse dynamics in the cavity are assumed to deviate by small factors from the soliton solution. In many mode-locked fiber lasers, these two underlying conditions do not necessarily hold because the nonlinear phase shift can be as high as several π per round

0740-3224/97/102681-10$10.00

trip, and the pulse can significantly deviate from the fundamental soliton solution. This limit has been previously considered in solid-state lasers, where the master mode-locking equation proved inadequate in describing the mode locking owing to strong nonlinearity and dispersion.[1,12,20,21] The effects of dispersion on mode-locked fiber lasers have also been extensively investigated experimentally and numerically.[22]

In this paper we present theoretical and numerical studies of a fiber laser mode locked by the SBR. The model, unlike the master mode-locking equation, is capable of treating significant intracavity pulse changes per round trip. A description of the pulse interaction with the SBR is also included. To our knowledge, this is the first time a direct comparison has been made between numerical and analytical results of a theoretical fiber-laser model with experimental results using no free parameters. The comparison is made for fiber lasers operating in both the normal and the anomalous dispersion regimes. Based on the excellent agreement between theory and experiment, this model provides a sound basis for understanding the contributions of various physical mechanisms, i.e., dispersion, nonlinearity, saturable absorption, to the mode-locking dynamics.

Our model begins with the nonlinear Schrödinger equation for propagation in fiber and applies to cases where the nonlinearities per round trip are large. We numerically solve the full propagation problem, including the leading-order dynamics of the SBR as a jump condition imposed every round trip. The SBR is modeled with three loss factors, which include its intrinsic loss, its fast and slow (saturating) responses, and a time constant to characterize the relaxation of the latter. The analytical model for the temporal response of the SBR matches closely the experimental measurements obtained with pump–probe experiments. Thus the mode-locking model provides a means to predict accurately the output temporal- and spectral-pulse profiles obtained experimentally. In addition, we derive an averaged model that captures the SBR dynamics and that may be solved analytically in a particular asymptotic regime.

This paper is organized as follows. In Section 2 the formulation of the general mode-locking equation is introduced. Section 3 describes the SBR model, which is utilized in determining the appropriate averaged-evolution equation described in Section 4. Section 5 considers analytic solutions to the averaged equation. In Section 6 the experimental results are presented and compared with numerical and analytic predictions. Conclusions are provided in Section 7.

2. FORMULATION

A pulse propagating in an optical fiber under the influence of the Kerr nonlinearity and including the effects of dispersion, loss, and a parabolic gain-bandwidth profile behaves according to the modified nonlinear Schrödinger (Ginzburg–Landau) equation:

$$i\frac{\partial Q}{\partial Z} + \frac{D}{2}\frac{\partial^2 Q}{\partial T^2} + \alpha|Q|^2 Q + i\Gamma Q - iG(Z)\left(1 + \tau\frac{\partial^2}{\partial T^2}\right)Q = 0. \quad (1)$$

Here Q is the normalized electric-field envelope and D, α, τ, and Γ denote the normalized dispersion, nonlinearity, gain bandwidth, and intrinsic loss, respectively. The variable T represents the physical time in the rest frame of the mode-locked pulse divided by an arbitrary reference time $T_0 = 1$ ps, and the variable Z represents the physical distance divided by the cavity round-trip length Z_{cav}. These scalings give the following parameter definitions

$$D = \frac{Z_{\mathrm{cav}}\lambda_0^2\bar{D}}{2\pi c T_0^2} \quad (2a)$$

$$\alpha = \frac{2\pi n_2|E_0|^2 Z_{\mathrm{cav}}}{\lambda_0 A_{\mathrm{eff}}} \quad (2b)$$

$$\tau = \frac{1}{\Omega^2 T_0^2} \quad (2c)$$

$$\Gamma = \tilde{\gamma} Z_{\mathrm{cav}}, \quad (2d)$$

where $n_2 = 2.6 \times 10^{-16}$ cm^2/W is the nonlinear coefficient in the fiber, $|E_0|^2 = 1$ kW is an arbitrary power scaling, $A_{\mathrm{eff}} = 60\ \mu$m^2 is the effective cross-sectional area of the fiber, $\tilde{\gamma} = 0.0230$ km^{-1}, which corresponds to a power-loss rate of 0.20 dB/km, Ω is the FWHM bandwidth of the fiber amplifier, and $\lambda_0 = 1.55\ \mu$m and c are the free-space wavelength and speed of light, respectively. The parameter $\bar{D}$ [in ps/(km nm)] gives the average normal ($\bar{D} < 0$) or anomalous ($\bar{D} > 0$) dispersion in the laser cavity. Note that this model differs from the experimental setup for which up to three fiber segments are utilized with differing dispersion values and effective cross-sectional areas (see Section 6). Here we have incorporated the effects of all three fiber segments into a single fiber medium (see Fig. 1). Although corrections to the average dispersion can be included, numerical and analytical[23–25] results suggest that they can be neglected with only a minimal amount of error incurred.

The gain in the fiber is incorporated through the dimensionless parameter $G = G(Z)$. We model the saturated gain in the fiber[15] by letting

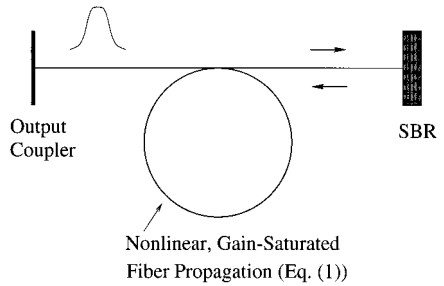

Fig. 1. Schematic of mode-locking fiber laser, which includes a 1% output coupler, SBR, and a gain-saturated fiber segment.

$$G(Z) = \frac{2G_0}{1 + \|Q(Z)\|^2/E_{\text{sat}}}, \tag{3}$$

where E_{sat} is the saturated energy of the fiber, G_0 is the saturated gain, and $\|Q(Z)\|^2 = \int_{-\infty}^{\infty}|Q(Z)|^2 dT$ is the current energy.

3. SATURABLE ABSORBER DYNAMICS

A comprehensive model of the SBR dynamics requires a description of the microscopic interactions between the intracavity radiation and the quantum-well structure and, consequently, extensive numerical modeling.[26] Here we simply incorporate the mode-locking action of the SBR through an empirical model of its nonlinear temporal response. The SBR structure, illustrated in Fig. 2, consists of a broadband AlAs–GaAs Bragg reflector and two uncoupled InGaAs–InP quantum wells separated by 7 nm and located 15 nm from the top surface of the sample. The complete structure has a ≈99.5% saturated reflectivity at 1.55 μm with a bandwidth of ≈150 nm, as shown in Fig. 2.

Since the optical field penetrates through only several micrometers in the SBR structure, we ignore the effects of the material dispersion in the Bragg reflector, and we model the steady-state SBR nonlinear reflectivity response as a jump condition attached to the propagation equation (1). The model includes a fast component representative of the virtual carrier transitions (AC Stark) and a slow component representative of the real transitions that incorporates a saturated term and a slow relaxation time.[27,28] Thus the combined response can be described by the jump condition

$$\begin{aligned} Q_+ = &\left(1 - \sigma_l - \sigma_f\left(1 - \frac{|Q_-|^2}{|Q_-|^2_{\max}}\right)\right. \\ &\left. - \sigma_s\left\{1 - \frac{\int_{-\infty}^{T}|Q_-|^2 dT}{\|Q_-\|^2}\right.\right. \\ &\left.\left. \times \exp\left[-H(T - T_{\max})\frac{T - T_{\max}}{T_d}\right]\right\}\right)Q_- \\ &= f(|Q|)Q_-, \end{aligned} \tag{4}$$

where $Q_\pm$ denotes the pulse before (−) and after (+) the SBR interaction, T_d is the decay time of the SBR slow response, which is normalized on T_0, σ_l is the intrinsic loss of the SBR, σ_f measures the relative strength of the instantaneous SBR response, and σ_s is the relative strength of the corresponding slow saturation response. Note that $|Q(T_{\max})| = |Q|_{\max}$ gives the power maximum and its relative position, and $H(T - T_{\max})$ is the standard Heaviside function[29] for which $H(T - T_{\max}) = 0$ for $T - T_{\max} < 0$ and $H(T - T_{\max}) = 1$ for $T - T_{\max} > 0$. Jump condition (4) is a phenomenological idealization of the steady-state interaction dynamics of the SBR with the electric field. Physically, the SBR is capable of responding only to the instantaneous power rather than to the integrated power ($\|Q\|^2$) and to the maximum power ($|Q|^2_{\max}$), as per Eq. (4).

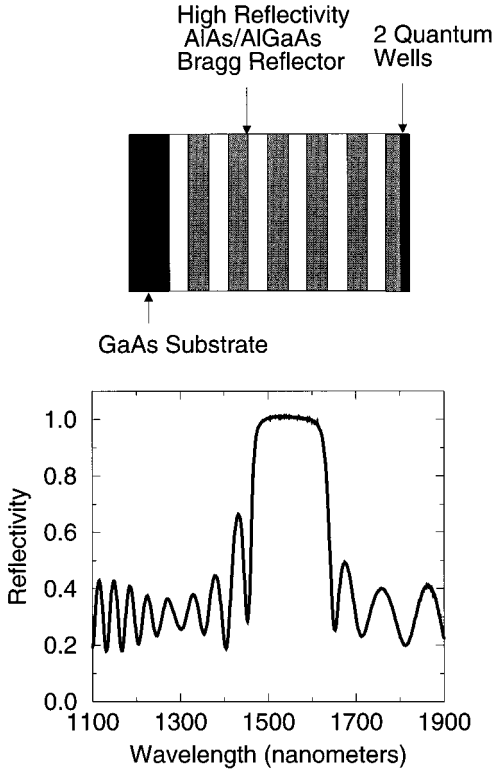

Fig. 2. SBR structure and its associated reflectivity spectrum.

In addition to the convenient mathematical description, Eq. (4) provides a qualitatively correct leading-order model for the SBR dynamics. Thus the SBR action is localized to the temporal window of the pulse, i.e., far from the pulse the radiation experiences only an ~2% absorption. This is in contrast to the master mode-locking equation[13] and soliton mode-locking models[19] for which radiation far from the localized pulse can be modeled correctly only if the pulse energy is known *a priori*.

The effect of the SBR can be illustrated by considering its action on a specific pulse. In particular, we consider the case for which $Q_- = \eta\ \text{sech}\, wT \exp[i\Theta(Z, T)]$. Plugging this initial ansatz into Eq. (4) gives the appropriate change in reflectivity of the SBR. In the case of a fast response acting alone ($\sigma_s = 0$, $\sigma_l = 0$), the change of reflectivity of the SBR is given by

$$\Delta_f = 1 - f(|Q|,\ \sigma_s = \sigma_l = 0) = \sigma_f \tanh^2 wT. \tag{5}$$

Similarly, the case of the slow response acting independently can be considered ($\sigma_f = 0$, $\sigma_l = 0$) and is found to give

$$\begin{aligned} \Delta_s = 1 - f(|Q|,\ \sigma_f = \sigma_l = 0) = &\frac{\sigma_s}{2} \\ &\times [2 - (1 + \tanh wT)\exp[-H(T)T/T_d)]. \end{aligned} \tag{6}$$

The fast and slow changes in reflectivity are plotted in Figs. 3(a) and 3(b), respectively, with $w = 1.76$, which corresponds to a 1-ps FWHM pulse, and $T_d = 14$ so that the SBR relaxation time is 14 ps.

In general, the SBR action will be some combination of the fast and slow responses, which depends primarily

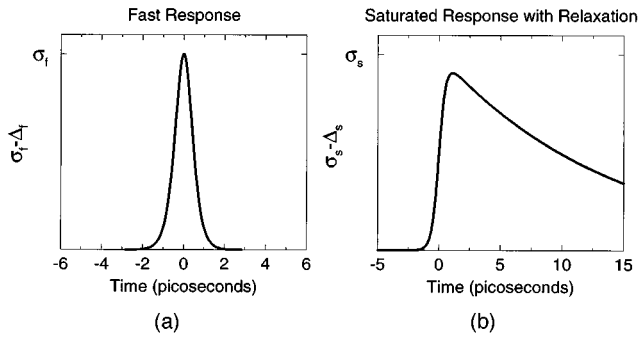

Fig. 3. (a) Change in reflectivity $\sigma_f - \Delta_f$ corresponding to the fast response. (b) $\sigma_s - \Delta_s$ gives the change in reflectivity that is due to the slow saturated response with relaxation. Note that Q_- corresponds to a 1-ps hyperbolic-secant pulse.

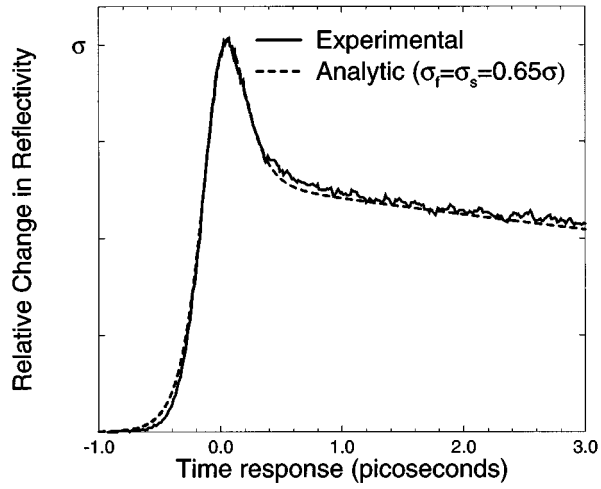

Fig. 4. Comparison of the experimental pump and probe measurements of the SBR at 1.55 μm with the jump condition of Eq. (7), which includes a fast response and slow saturation response with relaxation. Here, an ~400-fs hyperbolic-secant pulse is assumed for Q_-, and $\sigma_f = \sigma_s = 0.65\sigma$ with $T_d = 14$.

upon the relative position of the quantum-well exciton peak. In practice the quantum-well structures and their associated exciton peaks are designed around the desired wavelength of the mode-locking operation. Time resolved pump–probe measurements of the reflectivity have been made on the SBR sample at 1.55 μm. In this case it is observed that both slow and fast responses are present, so that for a (chirped) hyperbolic secant pulse we have

$$f(|Q|) = 1 - \sigma_l - \sigma_f \tanh^2 wT - \frac{\sigma_s}{2}\{2 - (1 + \tanh wT)\exp[-H(T)T/T_d]\}. \tag{7}$$

We can compare this simple model with the experimental findings obtained through pump–probe measurements. Figure 4 depicts the comparison between the experiment and the analytic results of Eq. (7) where w is chosen to match a ≈400-fs FWHM pulse, $T_d = 14$ (a 14-ps decay time), $\sigma_l = 0.005$ for a saturated reflectivity of 99.5%, and $\sigma_f = \sigma_s = 0.65\sigma$ where σ is the maximum change in reflectivity of the SBR. Note the excellent agreement in Fig. 4 between the simple analytic model given by Eq. (4) and the experimental results. We estimate from experiments that the maximum change in reflectivity is ~2%. This gives $\sigma = 2\%$ and $\sigma_f = \sigma_s = 1.3\%$. These parameter values for the SBR will be used in the numerical and analytical calculations that follow.

Before concluding this section, the range of validity of Eq. (4) should be discussed. We can expect the simple jump condition (4) to model the SBR dynamics only for well-behaved, near-steady-state mode locking, i.e., a single pulse per round-trip configuration. When multiple pulses or radiation pedestals appear, a more detailed understanding of the SBR dynamics will be required.

4. AVERAGED EVOLUTION

In the previous two sections the evolution dynamics of the pulse in the fiber and the leading-order effect of the SBR were considered. In this section we incorporate the SBR dynamics into propagation equation (1) for the pulse evolution in the fiber. The model derived is not simply a heuristic or qualitative model, but rather an asymptotically valid model for the nonlinear pulse dynamics. Thus a direct comparison among the averaged evolution, which resembles the usual master mode-locking equation (Ginzburg–Landau equation), the full dynamics given by Eqs. (1), (3), and (4), and the experiment can be made. Finally, it should be noted that averaging does not require the self-phase modulation to be small per round trip. Rather, the physically relevant case of a dominant nonlinearity (self-phase modulation) can be addressed.

The averaged evolution incorporates the effect of the SBR and the output coupler by implementing them continuously over the fiber segment. Since the SBR and the output coupler act as quasi-linear and linear loss terms, respectively, we can incorporate them into the propagation equation (1) through the simple linear model

$$\frac{\partial Q}{\partial Z} = \beta Z_{\text{cav}} Q. \tag{8}$$

Here we neglect the effects of dispersion, nonlinearity, bandwidth-limited fiber gain, and intrinsic fiber losses, and once again scale the physical distance on Z_{cav}. The solution to Eq. (8) is $Q(Z, T) = Q(0, T)\exp(\beta Z_{\text{cav}} Z)$.

To make use of Eq. (8) and its solution, we consider the propagation over a single round trip. We then equate the round-trip dynamics with an effective jump condition and compare this with Eq. (4). Thus, after a single round trip, $Z = 1$, and we find that $Q(1, T) = Q_+ = Q(0, T)\exp(\beta Z_{\text{cav}}) = Q_- \exp(\beta Z_{\text{cav}})$. Comparing the above relationship between Q_+ and Q_- with Eq. (4) gives

$$\exp(\beta Z_{\text{cav}}) = f(|Q|). \tag{9}$$

Solving for β in Eq. (9) yields $\beta Z_{\text{cav}} = \log[f(|Q|)]$. We can further approximate βZ_{cav} by noting that $\log(1 + \epsilon) = \epsilon + O(\epsilon^2)$, where $\epsilon \ll 1$. Since σ_l, σ_f, $\sigma_s \ll 1$, it follows from linearization that

$$\beta Z_{\mathrm{cav}} \approx -\sigma_l - \sigma_f\left(1 - \frac{|Q|^2}{|Q|^2_{\max}}\right) - \sigma_s\left\{1 - \frac{\int_{-\infty}^{T}|Q|^2 \mathrm{d}T}{\|Q\|^2} \times \exp\left[-H(T - T_{\max})\frac{T - T_{\max}}{T_d}\right]\right\}, \quad (10)$$

with an error, which is $O(\sigma_f^2, \sigma_s^2, \sigma_l^2)$.

Similarly, the output coupler can be incorporated into Eq. (8) by simply noting that the appropriate jump condition there is

$$Q_+ = RQ_-, \quad (11)$$

where R is the reflectivity of the output coupler. Thus the contribution from the output coupler gives

$$\beta Z_{\mathrm{cav}} \approx (1 - R), \quad (12)$$

which is derived again by comparing the relation between Q_+ and Q_- and noting that $(1 - R) \ll 1$.

By making use of Eq. (8), Eqs. (10) and (12) can be incorporated into the propagation equation (1) to give an averaged evolution equation for the pulse dynamics:

$$i\frac{\partial Q}{\partial Z} + \left[\frac{D}{2} - i\tau G(z)\right]\frac{\partial^2 Q}{\partial T^2} + i[\gamma - G(Z)]Q + \left(\alpha - i\frac{\sigma_f}{|Q|^2_{\max}}\right)|Q|^2 Q - i\sigma_s\frac{\int_{-\infty}^{T}|Q|^2 \mathrm{d}T}{\|Q\|^2} \times \exp\left[-H(T - T_{\max})\frac{T - T_{\max}}{T_d}\right]Q = 0, \quad (13)$$

where $\gamma = \Gamma + 1 - R + \sigma_l + \sigma_f + \sigma_s$. Equation (13) is similar to the master mode-locking equation. However, there are significant differences that are due to the addition of the slow response with relaxation, the fast-response scaling $\sigma_f/|Q|^2_{\max}$, and the contribution of linear parts in γ proportional to σ_l, σ_f, and σ_s.

Equation (13) is most accurate under the condition that the pulse amplitude and shape do not change significantly per round trip. Since the effects of dispersion and nonlinearity can distort the pulse profile considerably, we would ideally require $Z_{\mathrm{cav}}/Z_0 \ll 1$. This condition is easily met for the picosecond mode-locked pulses of the normal dispersion regime [$Z_{\mathrm{cav}}/Z_0 \approx O(10^{-3})$]. However, ultrashort pulses are generated in the anomalous dispersion regime for which $Z_{\mathrm{cav}}/Z_0 \approx 0.5$. Despite this, the agreement between the averaged evolution and full equations is remarkable. In addition, the conditions $\sigma_f, \sigma_s, (1 - R) \ll 1$ must hold for Eqs. (10) and (12) to apply. We note that these results differ from the previous derivation of the master mode-locked equation[15] for which all the parameters are required to be much less than unity per round trip.

5. PULSE SOLUTIONS

Equation (13) admits exact solutions in certain asymptotic parameter regimes. For the case in which the SBR response has no resonant (slow) response, i.e., $\sigma_s = 0$, chirped solutions take the form[30]

$$Q(Z, T) = \eta[\mathrm{sech}\, wT]^{1+iA}\exp[i\phi(Z)], \quad (14)$$

where the parameters ϕ and η are determined from the values of w and A by

$$\frac{\mathrm{d}\phi}{\mathrm{d}Z} = \frac{1}{2}Dw^2(1 - A^2) + 2\tau G_0 w^2 A, \quad (15a)$$

$$\eta^2 = \frac{w^2}{2\alpha}[D(2 - A^2) + 6\tau G_0 A], \quad (15b)$$

and the parameters w and A satisfy

$$Dw^2 A - [\tau w^2(1 - A^2) + 1]G_0 + \gamma = 0, \quad (16a)$$

$$3Dw^2 A - 2\tau G_0 w^2(2 - A^2) + 2\sigma_f = 0. \quad (16b)$$

Solving the system given by Eq. (16) gives the quadratic equation for A:

$$A^2(\sigma_f + B) + A\frac{D}{\tau G_0}\left(\sigma_f + \frac{3}{2}B\right) - (\sigma_f + 2B) = 0, \quad (17)$$

where $B = G_0 - \gamma$, and whose solution is

$$A_\pm = \frac{1}{\sigma_f + B}\left\{-\frac{D}{2\tau G_0}\left(\sigma_f + \frac{3}{2}B\right) \pm \left[\frac{D^2}{4\tau^2 G_0^2}\left(\sigma_f + \frac{3}{2}B\right)^2 + (\sigma_f + B)(\sigma_f + 2B)\right]^{1/2}\right\}. \quad (18)$$

Once A is determined we find

$$w_\pm^2 = \frac{2\sigma_f}{2\tau G_0(2 - A_\pm^2) - 3DA_\pm}, \quad (19)$$

and ϕ and η are determined from Eq. (15). Although two solution branches are given by Eq. (18), these solutions must be self consistent in that the right-hand sides of both Eqs. (15b) and (19) must be real and positive. It should be noted that chirped solution (14) of the Ginzburg–Landau equation arises in a wide variety of mode-locking configurations.[15,22,30]

We will not make parameter regime studies here. However, we will point out that nothing at this point can be said concerning the stability of the chirped hyperbolic-secant pulse solutions. A stability analysis of the pulse evolution requires a linearization about the chirped solution. This has been explored numerically for the master mode-locking equation,[31] but remains an open question analytically. These issues are currently under investigation and will be addressed elsewhere.

We also consider the case for which $\sigma_s \neq 0$. In this case there is no longer an exact solution of Eq. (13). However, in the physically relevant limit for which $\sigma_s \ll 1$, the slow-response term can be treated as a perturbation to the $\sigma_s = 0$ case. In particular, we examine the

case for which there is no relaxation (e.g., $T_d = \infty$) and consider the traveling-wave solution

$$Q(Z, T) = \eta[\text{sech } w(T - vZ)]^{1+iA} \exp[i\phi(Z)]. \tag{20}$$

As in the previous case with $\sigma_s = 0$, the parameters η, w, ϕ, and A satisfy Eqs. (15) and (16), with the additional restriction now that

$$v(1 + iA) = \frac{\sigma_s}{2w}[1 + \coth w(T - vZ)]. \tag{21}$$

Equation (21) cannot be satisfied unless $v = 0$ and $\sigma_s = 0$, i.e., the case of no slow response considered previously. However, for the case in which $v \ll 1$ and the $T - vZ \gg 1$ limit is considered, we find

$$v \approx \frac{\sigma_s}{w}. \tag{22}$$

So although no solutions exist, we obtain a crude estimate for the leading-order drift of the pulse.

In addition to the approximate traveling-wave solution found above, care must be taken when comparing the analytic solution with the numerical results of the full equation, which includes the slow response and relaxation. In particular, the value of σ_s in the definition of γ must be modified to account for the effective loss that is due to the slow response. Simply setting $\sigma_s = 0$ gives pulse solutions that are much too large because the value of G_0 calculated numerically takes into account the loss that is due to a nonzero σ_s. The effective slow response can be found by averaging the slow response in Eq. (6):

$$\bar{\sigma}_s = \frac{\sigma_s}{2(t_1 + t_2)} \int_{-t_1}^{t_2} \left\{ 2 - (1 + \tanh wt) \exp\left[-\frac{H(t)t}{T_d} \right] \right\} dt$$

$$\approx 0.65\sigma_s. \tag{23}$$

Here the limits of integration, t_1 and t_2, are chosen to capture the localized structure of the slow response and relaxation near the pulse [see Fig. 3(b)]. Note that if no relaxation were included, Eq. (23) would simply integrate to $\bar{\sigma}_s = 0.5\sigma_s$.

6. NUMERICS AND EXPERIMENTS

To verify the analytic predictions made in the preceding two sections, extensive numerical simulations are described in this section. The numerical method utilized employs a fourth-order Runge–Kutta method in space (Z) and a filtered pseudospectral method in time (T).[32] This procedure combines the advantages of split-step[33] and explicit Runge–Kutta[34] methods, giving a relatively simple fourth-order scheme with improved numerical stability.

For the simulations that follow we chose an unchirped hyperbolic secant pulse as the initial condition:

$$Q(0, T) = \eta_0 \text{ sech}(1.76 w_0 T). \tag{24}$$

Here η_0 and w_0 are the initial pulse amplitude and the inverse of the initial FWHM, respectively. We set $w_0 = 0.1$, which corresponds to a 10-ps pulse. The initial amplitude η_0 is then determined by the initial energy in the cavity. It should be noted that these initial conditions are arbitrary, as we have observed numerically that a very wide range of pulselike initial conditions mode lock to the same steady-state pulse solution.

We begin by considering the mode-locking pulse dynamics in the normal dispersion regime. For this case the experimental laser cavity consists of three fiber segments of lengths 13 cm, 19 cm, and 95 cm with dispersion values of 17.0 ps/(km nm), −9.1 ps/(km nm), and −51.6 ps/(km nm), respectively (see Fig. 5). Thus the cavity length is 127 cm ($Z_{\text{cav}} = 254$ cm) with an average cavity dispersion of $\bar{D} \approx -38$ ps/(km nm). It should be noted that the −9.1-ps/(km nm) (19-cm) segment is the erbium–ytterbium gain fiber. The saturated intracavity power measured experimentally is $E_{\text{sat}} = 21.3$ mW so that a value of $G_0 = 0.03256$ is required. Finally, we assume the erbium–ytterbium fiber has a 25-nm FWHM gain bandwidth and take $\eta_0 = 0.1144$ so that the initial energy is half the saturated energy of the cavity.

We begin by considering the full governing evolution as given by Eqs. (1), (4), and (11). In Fig. 6 we show the evolution over 1000 round trips of the fiber cavity. In Fig. 6(a) we observe that the pulse settles to a ≈13.5-ps (FWHM) pulse, which is consistent with experimental estimates. It is interesting to note the evolution of the spectrum in Fig. 6(b) as it evolves into a square shape in the frequency domain. This supports the notion of the formation of chirped-pulse structures alluded to in the previous section. The evolution of the pulse as governed by averaged equation (13) gives similar quantitative results.

To test the validity of the proposed evolution model and its various approximations, we compare the model predictions directly with experimental results. In Fig. 7 we compare the experimental output profiles with the steady-state (numerical) solution of the full governing equations [Eqs. (1), (4), and (11)], the averaged equation [Eq. (13)], and its exact solution [Eqs. (14)–(19) with σ_s replaced by $0.65\sigma_s$ as per Eq. (23)]. Note the excellent agreement among all four. In the time domain, for which we do not have an experimental autocorrelation trace, the pulse width is estimated to be just over 10 ps. This compares favorably with the theoretical predictions of ~13.5 ps.

In this case the parameters for the analytic solution given by Eq. (14) are calculated using Eq. (23) so that $\bar{\sigma}_s = 0.65\sigma_s = 0.00845$ and $\gamma = \Gamma + 1 - R + \sigma_l + \sigma_f + \bar{\sigma}_s$. Plugging in our parameter values yields η_+

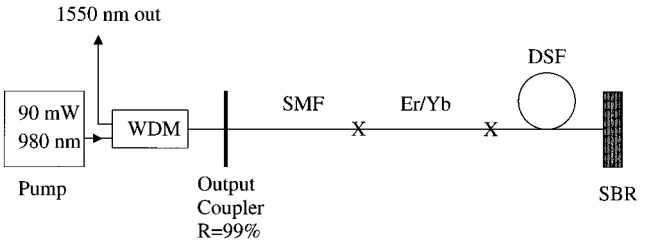

Fig. 5. Experimental setup of mode-locking laser cavity with a 1% output coupler, SBR, and average dispersion in the anomalous regime. The 980-nm pump is coupled through a wavelength division multiplexer (WDM) into the laser cavity, which consists of three fiber segments: a single-mode fiber (SMF), an erbium–ytterbium fiber (Er/Yb), and finally a dispersion-shifted fiber (DSF).

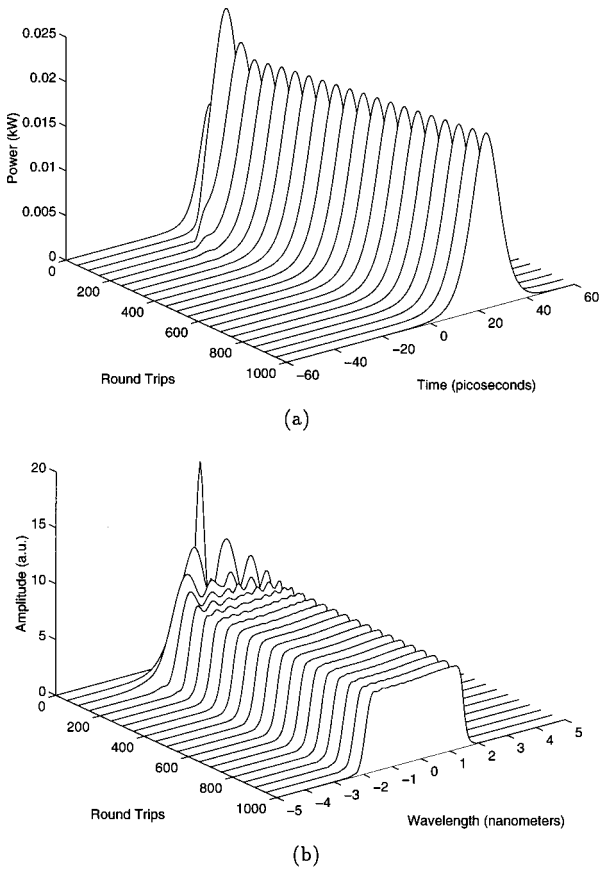

Fig. 6. Numerical simulation of the pulse evolution as governed by Eqs. (1), (4), and (11) in both (a) the time and (b) the frequency domain for a fiber cavity with an average normal dispersion value of $\bar{D} = -38.1$ ps/(km nm). In (a) the pulse is seen to mode lock to a ~13.6 ps chirped pulse whose spectral evolution is given by (b).

$= 0.1393$, $w_+ = 0.1128$, and $A_+ = 11.5204$ [the second solution branch of Eq. (18) is not self consistent in that it yields imaginary values for w_- and η_-]. This confirms the validity of the asymptotic approximations made in deriving averaged equation (13) and further helps illuminate the usefulness of the analytic solution given by Eq. (14) in determining the range of operation of the fiber laser even when the slow response with relaxation is present.

Similarly, we can consider the case for which the average dispersion in the fiber laser is in the anomalous regime. Again the laser cavity comprises three fiber segments of length 24 cm, 17 cm, and 49 cm with dispersion values of 17.0 ps/(km nm), −9.1 ps/(km nm) and 17.0 ps/(km nm), respectively. The cavity length is then 90 cm ($Z_{\text{cav}} = 180$ cm) with an average dispersion value of $\bar{D} \approx 12$ ps/(km nm). In this case the output coupling is 2%, and the intracavity power is estimated from measurements to be ≈10 mW. Here we chose η_0 and w_0 so that initially we have a 1-ps pulse with the exact initial energy of the saturated cavity. In addition, we take an effective fiber bandwidth (FWHM) of ~45 nm. Although this bandwidth is broader than that of the 20–25-nm erbium–ytterbium fiber, it is a reasonable assumption given that the pulse propagates a majority of the time in essentially bandwidth-unlimited fiber. Thus the larger bandwidth allows the self-phase modulation to have a stronger broadening effect in the fiber cavity. All other parameters, including $\sigma_f = \sigma_s = 1.3\%$ and $\sigma_l = 0.5\%$, remain as in the normal dispersion case.

In Fig. 8 we show the evolution as given by Eqs. (1), (4), and (11) over 1000 round trips of the fiber cavity for the parameter values given in the previous paragraph. In Fig. 8(a) we observe that after several hundred round trips, the pulse settles to a ~500-fs (FWHM) pulse. In contrast with the spectral evolution of the normal dispersion case, the spectrum in Fig. 8(b) evolves into a broadband pulse in the frequency domain. The experimental time–bandwidth calculation yields a value of ~0.4 so that the pulse is nearly bandwidth limited [i.e., $A \ll 1$ in Eq. (14)]. The evolution of averaged equation (13) gives similar quantitative results as those in Fig. 8.

The validity of the proposed evolution model and its various approximations are once again tested by comparing predictions directly to experimental results. We can calculate the analytic solution of the averaged equation [Eqs. (14)–(19) with Eq. (23)] given the appropriate parameters. Calculating the chirped-soliton parameters gives $\eta_+ = 0.2858$, $w_+ = 2.9789$, and $A_+ = 0.1566$ ($\ll 1$).

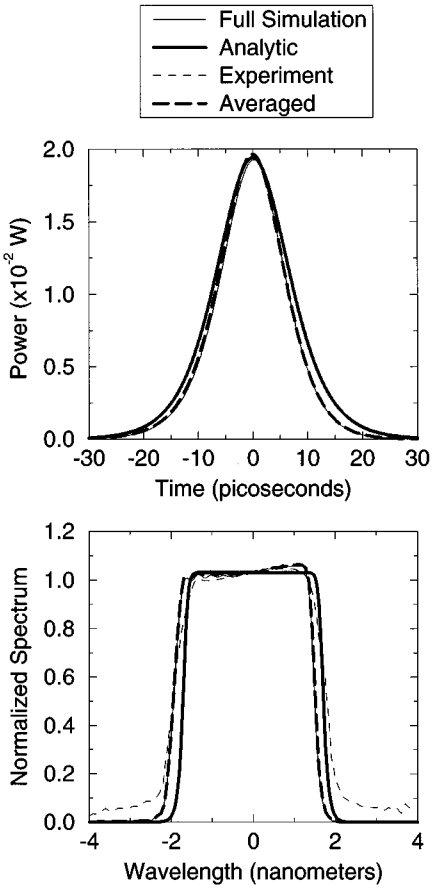

Fig. 7. Comparison of the experimental results with $\bar{D} \approx -38$ ps/(km nm) and the full evolution equations [Eqs. (1), (4), and (11)], the averaged equation [Eq. (13)], and the approximate solution with no slow response [Eqs. (14)–(19)]. Note the remarkable agreement between all three models and the experimental results. The 13.5-ps pulse width is consistent with experimental observation.

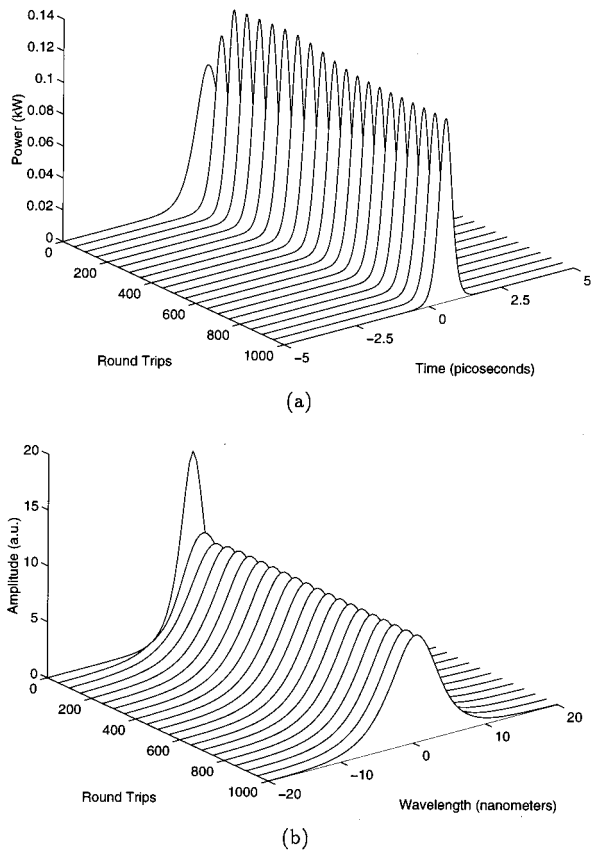

Fig. 8. Numerical simulation of the pulse evolution as governed by Eqs. (1), (4), and (11) in both (a) the time and (b) the frequency domain for a fiber cavity with an average anomalous dispersion value of $\bar{D} \approx 12$ ps/(km nm). In (a) the laser is seen to mode lock to an ~420-fs chirped pulse with a time–bandwidth product of ~0.4 and whose spectral evolution is given by (b).

Thus a slightly chirped pulse is indeed the steady-state solution. As before, the second branch of these solutions yields an imaginary value for η_-. In Fig. 9 we compare the experimental output profiles with the steady-state (numerical) solution of the full governing equations [Eqs. (1), (4), and (11)], the averaged equation [Eq. (13)], and the analytical chirped solution. These results once again confirm the validity of the asymptotic approximations made in deriving averaged equation (13) and further demonstrate the usefulness of solutions (14)–(19).

Finally, we simulate the pulse evolution as governed by Eqs. (1), (4), and (11) for the case in which we double the cavity length. Thus we have an intracavity power of ~10 mW, a bandwidth of 25 nm, and a cavity of length ~180 cm ($Z_{\text{cav}} = 360$ cm) with average dispersion $\bar{D} \approx 12$ ps/(km nm). In this simulation, we assume the strongest mode locking possible by allowing the SBR response to be purely instantaneous. This is also chosen so that the multiple-pulsing behavior observed numerically no longer contains a slow response since the slow response as given by Eq. (4) is completely unphysical in this multiple-pulsing regime. Thus we take $\sigma_s = 0.0$ and $\sigma_f = 2.6\%$. Figure 10 depicts the time evolution of the pulse through just 30 round trips. Note that the pulse begins to evolve in a complicated fashion and appears to be breaking up into a chain of solitary waves. This is most likely due to the length of the cavity, which allows the build up of self-phase modulation that can no longer be overcome by the intensity-dependent loss of the SBR. This multiple-pulse dynamics has been observed experimentally but has not yet been fully quantified. It will be

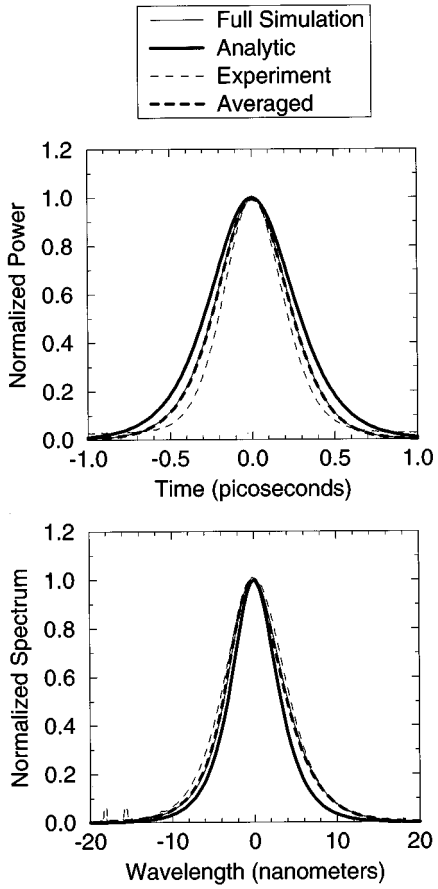

Fig. 9. Comparison of the experimental autocorrelation measurements (scaled with the assumption that the pulse shape is a hyperbolic secant) and output spectrum with the full evolution equations [Eqs. (1), (4), and (11)], the averaged equation [Eq. 13)], and the approximate analytic solution with no slow response [Eqs. (14)–(19)].

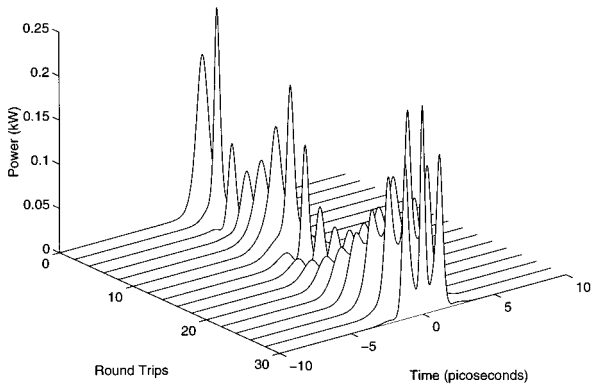

Fig. 10. Typical evolution of a pulse governed by full evolution equations (1), (4), and (11) in the anomalous dispersion regime $\bar{D} \approx 12$ ps/(km nm). Note that for the estimated experimental parameter values the pulse begins to break up into a group of multiple pulses. In this simulation we have taken $\sigma_s = 0$ and $\sigma_f = 2.6\%$.

explored further elsewhere. It should be noted that similar dynamics have been previously observed in Ginzburg–Landau evolution equations.[22]

7. CONCLUSIONS

We have developed a theory for the mode-locking pulse dynamics in a fiber laser with a saturable Bragg reflector (SBR). The theory applies in both the normal and the anomalous dispersion regimes and provides a model that has been compared directly with experimental results. Quantitative agreement is achieved in both dispersion regimes.

The theoretical model begins with the propagation equations in the fiber cavity, with appropriate jump conditions imposed at the cavity ends where the SBR and the output coupler are placed. The full evolution is approximated by folding the SBR and the output-coupler dynamics into the governing equations, and an averaged equation is derived. In the limit of no slow response and relaxation for the SBR, the averaged equation yields exact chirped-pulse solutions. Each level of approximation is asymptotically justified and shown to be relevant for the experimental parameters used here. In addition, comparison is made between the three levels of approximations and the experiment.

In this fiber-laser configuration the mode-locking dynamics are shown to be strongly driven by the fast AC-Stark shift[27] of the quantum wells on the Bragg reflector structure. This allows mode locking of pulses as short as 400 fs in the anomalous dispersion regime. Pump–probe measurements confirm the existence of the instantaneous AC Stark. It should be noted that stable mode locking occurs when the pulse spectrum lies just below the excitonic bandgap, where the AC-Stark shift is strongest. In addition to the instantaneous fast response, which is the primary mechanism for mode locking, the slow response and relaxation of the SBR are shown to cause a pulse drift and slight asymmetrization of the pulse. We emphasize that this SBR model accurately treats the radiation far from the localized pulse so that only $\sim 2\%$ at most is absorbed. In contrast, the master equation,[15] and thereby the soliton mode-locking model, fails to correctly capture this physical response of the semiconductor saturable absorber unless the pulse energy is known *a priori*. Our model suggests that the ideal mode-locking mechanism is a purely instantaneous response, which both stabilizes the mode-locked pulse and attenuates the dispersive radiation.

The mode-locking theory presented here extends beyond the qualitative description of the master mode-locking equation. We provide a quantitative model that can be utilized as a powerful design tool in evaluating the performance of fiber lasers mode locked in the normal and anomalous dispersion regimes.

ACKNOWLEDGMENTS

We thank James P. Gordon for several valuable discussions, M. Koch for the experimental pump–probe measurements of Fig. 4, and W. Y. Jan, R. Pathak, and J. E. Cunningham for the SBR sample. J. N. Kutz and P. Holmes acknowledge support from a National Science Foundation University-Industry postdoctoral fellowship (DMS-9508634). K. Bergman acknowledges support from the National Science Foundation (ECS-9502491) and the U. S. Office of Naval Research (N00014-96-0773). P. Holmes acknowledges additional support from the Department of Energy (DE-FG02-95ER.25238.A000), and M. Weinstein acknowledges support from the National Science Foundation (DMS-9500997).

*J. Nathan Kutz is also with Lucent Technologies and AT&T Research, Murray Hill, New Jersey 07974. Contact by e-mail, kutz@math.princeton.edu; telephone, 609-258-6495; fax, 609-258-1735.

†Permanent address: Department of Mathematics, University of Michigan, Ann Arbor, Michigan 48109.

REFERENCES

1. I. N. Duling III and M. L. Dennis, *Compact Sources of Ultrashort Pulses* (Cambridge University, Cambridge, England, 1995).
2. I. N. Duling III, "Subpicosecond all-fiber erbium laser," Electron. Lett. **27**, 544–545 (1991).
3. D. J. Richardson, R. I. Laming, D. N. Payne, V. J. Matsas, and M. W. Phillips, "Self-starting, passively modelocked erbium fiber laser based on the amplifying Sagnac switch," Electron. Lett. **27**, 542–544 (1991).
4. M. L. Dennis and I. N. Duling III, "High repetition rate figure eight laser with extracavity feedback," Electron. Lett. **28**, 1894–1896 (1992).
5. K. Tamura, H. A. Haus, and E. P. Ippen, "Self-starting additive pulse modelocked erbium fiber ring laser," Electron. Lett. **28**, 2226–2228 (1992).
6. M. E. Fermann, M. J. Andrejco, Y. Silverberg, and M. L. Stock, "Passive modelocking by using nonlinear polarization evolution in a polarizing-maintaining erbium-doped fiber," Opt. Lett. **18**, 894–896 (1993).
7. E. A. DeSouza, C. E. Soccolich, W. Pleibel, R. H. Stolen, M. N. Islam, J. R. Simpson, and D. J. DiGiovanni, "Saturable absorber modelocked polarization maintaining erbium-doped fiber laser," Electron. Lett. **29**, 447–449 (1993).
8. S. Tsuda, W. H. Knox, J. L. Zyskind, J. E. Cunningham, W. Y. Jan, and R. Pathak, "Broadband compact mode-locked Er/Yb fiber laser," in *Conference on Lasers and Electro-Optics*, Vol. 9 of OSA Technical Digest Series (Optical Society of America, Washington, D.C., 1996), paper CFD2.
9. S. Tsuda, W. H. Knox, E. A. de Souza, W. Y. Jan, and J. E. Cunningham, "Low-loss intracavity AlAs/AlGaAs saturable Bragg reflector for femtosecond modelocking in solid-state lasers," Opt. Lett. **20**, 1406–1408 (1995).
10. B. C. Collings, J. B. Stark, S. Tsuda, W. H. Knox, J. E. Cunningham, W. Y. Jan, R. Pathak, and K. Bergman, "Saturable Bragg reflector self-starting passive mode locking of a Cr^{4+}:YAG laser pumped with a diode-pumped Nd:YVO_4 laser," Opt. Lett. **21**, 1171–1173 (1996).
11. F. X. Kartner, L. R. Brovelli, D. Kopf, M. Kamp, I. Calasso, and U. Keller, "Control of solid-state laser dynamics by semiconductor devices," Opt. Eng. **34**, 2024–2036 (1995).
12. F. Krausz, M. E. Fermann, T. Brabec, P. F. Curley, M. Hofer, M. H. Ober, C. Speilmann, E. Wintner, and A. J. Schmit, "Femtosecond solid-state lasers," IEEE J. Quantum Electron. **28**, 2097–2122 (1992).
13. H. A. Haus, J. G. Fujimoto, and E. P. Ippen, "Analytic theory of additive pulse mode-locking and Kerr lens modelocking," IEEE J. Quantum Electron. **28**, 2086–2096 (1992).
14. H. A. Haus, E. P. Ippen, and K. Tamura, "Additive pulse modelocking in fiber lasers," IEEE J. Quantum Electron. **30**, 200–208 (1994).
15. H. A. Haus, J. G. Fujimoto, and E. P. Ippen, "Structures for additive pulse mode locking," J. Opt. Soc. Am. B **8**, 2068–2076 (1991).

16. M. Hofer, M. H. Ober, F. Haberl, and M. E. Fermann, "Characterization of ultrashort pulse formation in passively modelocked fiber lasers," IEEE J. Quantum Electron. **28**, 720–728 (1992).
17. H. A. Haus and A. Mecozzi, "Noise of mode-locked lasers," J. Lightwave Technol. **29**, 983–996 (1993).
18. S. M. J. Kelly, K. Smith, K. J. Blow, and N. J. Doran, "Averaged soliton dynamics of high-gain erbium fiber laser," Opt. Lett. **16**, 1337–1339 (1991).
19. F. X. Kärtner, D. Kopf, and U. Keller, "Solitary pulse stabilization and shortening in actively modelocked lasers," J. Opt. Soc. Am. B **12**, 486–496 (1994).
20. T. Brabec, C. Spielmann, and F. Krausz, "Limits of pulse shortening in solitary lasers," Opt. Lett. **17**, 748–750 (1992).
21. P. F. Curley, C. Spielmann, T. Brabec, E. Winter, and F. Krausz, "Periodic pulse evolution in solitary lasers," J. Opt. Soc. Am. B **10**, 1025–1028 (1993).
22. M. Romagnoli, S. Wabnitz, P. Franco, M. Midrio, L. Bossalini, and F. Fontana, "Role of dispersion in pulse emission from a sliding-frequency fiber laser," J. Opt. Soc. Am. B **12**, 938–944 (1995).
23. A. Hasegawa and Y. Kodama, "Guiding-center soliton in fibers with periodically varying dispersion," Opt. Lett. **16**, 1385–1387 (1991).
24. J. C. Bronski and J. N. Kutz, "Guiding-center pulse dynamics in nonreturn-to-zero (return-to-zero) communications system with mean-zero dispersion," J. Opt. Soc. Am. B **14**, 903–911 (1997).
25. J. C. Bronski and J. N. Kutz, "Asymptotic behavior of the nonlinear Schrödinger equation with rapidly-varying, mean-zero dispersion," Physica D **108**, 315–329 (1997).
26. H. Haug and S. W. Koch, *Quantum Theory of the Optical and Electronic Properties of Semiconductors*, 3rd ed. (World Scientific, Singapore, 1994), Chap. 16, pp. 317–327.
27. D. S. Chemla, W. H. Knox, D. A. B. Miller, S. Schmitt-Rink, J. B. Stark, and R. Zimmermann, "The excitonic optical Stark effect in semiconductor quantum wells probed with femtosecond optical pulses," J. Lumin. **44**, 233–246 (1989).
28. D. A. B. Miller, "Quantum well optical switching devices," in *Confined Electrons and Photons*, E. Burnstein and C. Weisbuch, eds. (Plenum, New York, 1995), pp. 675–701.
29. Erich Zauderer, *Partial Differential Equations of Applied Mathematics*, 2nd ed. (Wiley, New York, 1989), Chap. 7, pp. 426–446.
30. N. R. Pereira and L. Stenflo, "Nonlinear Schrödinger equation including growth and damping," Phys. Fluids **20**, 1733–1734 (1977).
31. C.-J. Chen, P. K. A. Wai, and C. R. Menyuk, "Stability of passively mode-locked fiber lasers with fast saturable absorption," Opt. Lett. **19**, 198–200 (1994).
32. T. Y. Hou, J. S. Lowengrub, and M. J. Shelley, "Removing the stiffness from interfacial flows with surface tension," J. Comput. Phys. **114**, 312–338 (1994).
33. M. D. Fleit and J. A. Fleck, "Light propagation in graded-index optical fibers," Appl. Opt. **17**, 3990–3998 (1978).
34. T. R. Taha and M. J. Ablowitz, "Analytical and numerical aspects of certain nonlinear evolution equations. II. Numerical, nonlinear Schrödinger equation," J. Comput. Phys. **55**, 203–230 (1984).